Brief Communication

MOLECULAR METABOLISM

PRDX1 Cys52Ser variant alleviates nonalcoholic steatohepatitis by reducing inflammation in mice

Zhonghao Bai [1,4], Wen Yin [1,4], Rui Liu [1], Minglei Tang [1], Xiaofeng Shi [1], Cheng Luo [2,3], Xiangyang Xie [1,*]

ABSTRACT

Objective: Peroxiredoxin 1 (PRDX1) is a peroxidase and guards against oxidative stress by scavenging intracellular peroxides, whereas it also has been shown to stimulate inflammatory response by functioning as a chaperone protein. The potential *in vivo* link between PRDX1's peroxidase activity and its pro-inflammatory activity remains elusive.

Methods: We generated peroxidase-dead PRDX1 variant mice by mutating its peroxidatic cysteine at 52 (Cys52) to serine, here referred to as PRDX1^{Cys52Ser}. Trx-TrxR-NADPH coupled activity assay was applied to evaluate the peroxidase activity of global PRDX in PRDX1^{Cys52Ser} variant mice. PRDX1^{Cys52Ser} mice and their wild-type littermates were subjected to western diet or methionine and choline deficient diet feeding. NASH phenotypes were assessed through different analyses including physiological measurements, immunohistochemical staining, and quantitative PCR (qPCR). RNA sequencing, qPCR and western blotting were used to reveal and validate any changes in the signaling pathways responsible for the altered NASH phenotypes observed between WT and PRDX1^{Cys52Ser} variant mice.

Results: PRDX1^{Cys52Ser} variant mice showed impaired global PRDX peroxidase activity and reduced susceptibility to diet-induced NASH and liver fibrosis. Mechanistically, PRDX1 Cys52Ser variant suppressed NF-κB signaling and STAT1 signaling pathways that are known to promote inflammation and NASH.

Conclusion: The peroxidatic Cys52 of PRDX1 is required for its pro-inflammatory activity *in vivo*. This study further suggests that PRDX1 may play dual but opposing roles in NASH.

© 2023 The Authors. Published by Elsevier GmbH. This is an open access article under the CC BY-NC-ND license (http://creativecommons.org/licenses/by-nc-nd/4.0/).

Keywords PRDX1; NASH; Inflammation; Cys52; NF-κB; STAT1

1. INTRODUCTION

Non-alcoholic steatohepatitis (NASH) is a more advanced form of non-alcoholic fatty liver disease (NAFLD) as the most common chronic liver disease worldwide and may progresses to cirrhosis and hepatocellular carcinoma [1]. The exact etiology of NASH remains complex or even to be debated [2]; however, several prominent events have been generally considered to be pathogenically driving NASH, which include lipotoxicity, inflammation and oxidative stress [1–5]. Thus, targeting these individual events could be potential therapeutic strategies for NASH treatment [2].

Peroxiredoxin 1 (PRDX1) belongs to a mammalian peroxidase family composed of six members that scavenge the majority of intracellular peroxides [6–9]. PRDX1 is a typical 2-Cys peroxidase containing a conserved cysteine residue at 52 (Cys52, known as peroxidatic cysteine) and a resolving cysteine residue at 173 (Cys173) [9]. When PRDX1 scavenges hydrogen peroxide (H_2O_2), oxidized Cys52 forms a disulfide-bond with Cys173 from another PRDX1 unit, consequently forming an inactive homo-dimer that can be further reduced back to the active monomer by thioredoxin (Trx) [9,10]. By this means, PRDX1 continuously exerts its peroxidase function to eliminate toxic H_2O_2.

A large body of evidence has well established the protective roles of PRDX1 through its peroxidase activity in guarding against oxidative stress in a variety of human diseases including cancer [11], ageing [12], atherosclerosis [13], and liver injury [14]. Surprisingly, however, PRDX1 has also been reported to promote inflammatory response and aggravate liver injury by functioning as a secreted chaperone protein [15,16]. Moreover, PRDX family members have been shown to initiate post-ischemic inflammation in the brain though their chaperon function [17], which is thought to be independent of their peroxidase activity [9,18]. Nonetheless, one previous *in vitro* study suggested that PRDX1's pro-inflammatory effect is dependent of its redox status [19]. Thus, the relationship between PRDX1's peroxidase activity and pro-inflammatory activity remains unclear.

Here, we aimed to investigate a potential connection between PRDX1's peroxidase activity and its pro-inflammatory effect by generating PRDX1^{Cys52Ser} variant mice. These variant mice showed impaired peroxidase activity as expected and alleviated diet-induced NASH

[1]NHC Key Laboratory of Hormones and Development, Tianjin Key Laboratory of Metabolic Diseases, Chu Hsien-I Memorial Hospital & Tianjin Institute of Endocrinology, Tianjin Medical University, Tianjin 300134, China [2]Zhongshan Institute for Drug Discovery, Shanghai Institute of Materia Medica, Chinese Academy of Sciences, Zhongshan 528437, China [3]School of Pharmaceutical Science and Technology, Hangzhou Institute for Advanced Study, University of Chinese Academy of Sciences, Hangzhou 310000, China

[4] Zhonghao Bai and Wen Yin contributed equally to this work.

*Corresponding author. 6 North Huanrui Road, Beichen District, Tianjin 300134, China. E-mail: xyxie@tmu.edu.cn (X. Xie).

Received March 22, 2023 • Revision received August 3, 2023 • Accepted August 4, 2023 • Available online 9 August 2023

https://doi.org/10.1016/j.molmet.2023.101789

 © 2023 The Authors. Published by Elsevier GmbH. This is an open access article under the CC BY-NC-ND license (http://creativecommons.org/licenses/by-nc-nd/4.0/).

phenotypes by suppressing NF-κB signaling and STAT1 signaling pathways. Our study provides *in vivo* evidence that peroxidatic Cys52 of PRDX1 is prerequisite for its pro-inflammatory activity and further suggests that PRDX1 plays dual but opposing roles in NASH.

2. METHODS

2.1. Animals

All mice used in the study contain C57BL/6J background, are housed at an animal facility core with stable temperature (22 °C), humidity and a 12/12 h light/dark cycle, and have free access to food and water. C57BL/6J mice were obtained from GemPharmatech (Nanjing, China). PRDX1^{Cys52Ser} variant mice were generated by GemPharmatech (Nanjing, China) through CRISPR—Cas9 technique. The gRNA sequences used for generation of PRDX1^{Cys52Ser} variant mice: CCACAGAAGCGCCAATCACT, CCAAGTGATTGGCGCTTCTG.

Eight-week-old mice (male or female) were fed a western diet (WD, Research Diets, D09100310, 40 kcal% Fat, 20 kcal% Fructose and 2% Cholesterol) for 20 weeks or a methionine and choline deficient diet (MCD, MolDietes, M0421) for 5 weeks to induce nonalcoholic steatohepatitis (NASH).

To evaluate hepatic NF-κB signaling activity, 8-week-old male WT and PRDX1^{Cys52Ser} variant mice on normal chow diet were intraperitoneally injected with LPS (10 mg/kg body weight) for 15 min before their livers were harvested for WB analysis.

All animal procedures were approved by the Animal Care and Use Committee at Chu Hsien-I Memorial Hospital & Tianjin Institute of Endocrinology, Tianjin Medical University. Both male and female mice were used for NASH phenotypic and biochemical analyses.

2.2. Primary mouse hepatocyte isolation and culture

Primary mouse hepatocytes were isolated from the livers of 6-week-old male WT and PRDX1^{Cys52Ser} mice on chow diet as previously described [20]. In brief, after anesthesia with isoflurane, the mouse liver was perfused sequentially with Krebs buffer containing EGTA and Krebs buffer containing $CaCl_2$ and collagenase type IV through the portal vein. The liver was dissected and hepatocytes were collected with ice-cold RPMI 1640, followed by filtration through a nylon filter. Afterward, primary hepatocytes were washed with ice-cold RPMI 1640 for 3 times to remove the remaining collagenase, evaluated for their viability (usually more than 85%) by trypan blue exclusion test, counted and seeded in collagen-coated plates. Primary hepatocytes were cultured and maintained in RPMI 1640 medium containing 10% FBS, 50 U/ml penicillin and 50 μg/ml streptomycin.

To evaluate the NF-κB signaling activity, primary mouse hepatocytes from WT and PRDX1^{Cys52Ser} mice were incubated with Hanks' balanced salt solution (HBSS) for 30 min, followed by LPS (500 ng/ml) stimulation for 15 min. To assess the expression of pro-inflammatory genes, primary mouse hepatocytes from WT and PRDX1^{Cys52Ser} mice were cultured in serum-free RPMI 1640 and treated with LPS (100 ng/ml) for 6 h [21].

2.3. Physiological measurements

Body weight and food intake measurements were performed as previously described [22]. Promethion High-Definition Multiplexed Respirometry System (Sable Systems, North Las Vegas, NV, USA) was applied to monitor mouse metabolism including oxygen consumption rate (VO_2), production rate of carbon dioxide (CO_2) (VCO_2) and locomotion activities.

2.4. Measurement of serum aspartate aminotransferase (AST) and alanine aminotransferase (ALT)

30 min after blood collection without addition of anticoagulant, the blood samples were centrifuged to collect serum. Serum levels of AST and ALT were analyzed with an automatic blood biochemical analyzer (AU680, Beckman Coulter).

2.5. Histological staining

Histological staining of mouse liver samples was prepared as previously described [23]. Briefly, mouse liver samples were fixed in freshly-made 4% paraformaldehyde (PFA) solution for 48 h, followed by a thorough washing with 1×PBS solution. Liver samples were embedded in paraffin and then sectioned for H&E, Sirius Red, or α-SMA staining.

For H&E and Sirius Red staining, specific kits from Solarbio (Beijing, China) were used according to the manufacturer's instructions. For α-SMA staining, a rabbit primary antibody against α-SMA (14395-1-AP, Proteintech), a polymer-HRP anti-rabbit secondary antibody and DAB (3,3′-diaminobenzidine) stain (PK10006, Proteintech) were employed. For Oil Red O staining (SHBL 1039, Sigma), fresh liver samples were immediately frozen and embedded in OCT (SAKURA), and later used for preparation of cryosection (8 μm).

An Olympus microscope equipped with different objective lenses was used to capture images.

2.6. Measurement of PRDX peroxidase activity

The peroxidase activity of global hepatic PRDX was measured as previously described [24] with some modifications. In brief, liver samples were homogenized in 50 mM HEPES-NaOH buffer (pH 7.0) including 0.2% Triton X-100 and protease inhibitors. To measure the global PRDX peroxidase activity, 200 μM NADPH, 3 μM recombinant Trx, and 1.5 μM TrxR were added to 100 μg of protein sample. The reaction was initiated by addition of H_2O_2 (50 μM) at 30 °C, immediately followed by detection of absorbance at 340 nm (A_{340}) for 15 min. In the meantime, the background activity was assessed in liver lysate with only NADPH, but without Trx and TrxR.

For initial rate calculation, a smooth curve was drawn through A_{340} readings, and the initial NADPH consumption rate (initial rate) was calculated by performing a simple linear regression using A_{340} readings during the first five minutes. The global PRDX peroxidase activity was calculated by subtracting the background activity (initial rate) from total activity (initial rate).

2.7. Quantitative PCR (qPCR)

qPCR was performed and quantified as previously described [22]. In brief, mouse liver tissues were homogenized in TRIzol (Invitrogen) and total RNA was extracted. 1 μg of RNA was used for reverse transcription, followed by qPCR using QuantStudio 3 Real-Time PCR System (Applied Biosystems). The relative expression levels of interest genes were quantified by $2^{-\Delta\Delta Ct}$ method using 36b4 as the reference gene. The qPCR primers used in the study was listed in Table S1.

2.8. Western blotting (WB)

Protein samples were prepared as previously described [22,25]. In brief, liver tissues were homogenized in 1× lysis buffer containing 1% deoxycholic acid, 10 mM $Na_4P_2O_7$, 1% Triton 100, 100 mM NaCl, 5 mM EDTA, 50 mM Tris—HCl and 0.1% SDS. Protein concentrations were determined with a BCA Protein Assay kit (23228; 23224, Thermo Fisher Scientific, Rockford, IL, USA). In general, a total of 20 μg of

 © 2023 The Authors. Published by Elsevier GmbH. This is an open access article under the CC BY-NC-ND license (http://creativecommons.org/licenses/by-nc-nd/4.0/).

protein was loaded in SDS-PAGE and transferred to PVDF membranes. The membranes were first blocked with 5% nonfat milk in 1XTBST, and then incubated with primary antibodies against PRDX1 (8499, Cell Signaling Technology, Danvers, MA, USA), Peroxiredoxin-SO3 (ab16830, abcam), phospho-NF-κB p65 (3033, Cell Signaling Technology), NF-κB p65 (8242, Cell Signaling Technology), Phospho-STAT1 (9167, Cell Signaling Technology), STAT1 (9145, Cell Signaling Technology), and Actin (A5441, Sigma) overnight at 4 °C, followed by incubation with secondary antibodies for 1 h at RT. Finally, an ECL detection system was used to develop signals.

2.9. Measurement of malondialdehyde (MDA) levels

To measure lipid peroxidation levels, we employed a commercial MDA detection kit (Beyotime Biotechnology, China) to measure MDA levels following the manufacturer's instructions. Briefly, we mixed liver lysate with MDA detection buffer and heated the mixture at 100 °C for 10 min, followed by the centrifuge at 1000 × *g* for 10 min. The supernatant was collected and then used for detection of absorbance at 535 nm (A_{535}) by a fluorometer (BioTek). Finally, MDA concentrations were normalized by protein concentrations.

2.10. HKPerox-Red staining in liver sections

Liver samples were frozen and embedded in OCT compound (SAKURA) in liquid nitrogen. Liver sections were prepared at the thickness of 8 μm for HKPerox-Red staining [26]. Briefly, liver sections were incubated with 5 μM HKPerox-Red in PBS (0.1% DMF (Macklin) and 100 mM CCl_3CN (Macklin)) for 10 min at room temperature. An Olympus fluorescence microscope with 40× objective lens was used to capture images. Image J was used to quantify the fluorescence intensity of images, and the data were processed by GraphPad Prism 9.

2.11. Transcriptome analysis

Liver samples were collected and stored in RNAlater (Ambion, TX, USA). Total RNA was isolated and purified for transcriptome analysis by LC-Bio Technology (Hangzhou, China). In brief, RNA was isolated with TRIzol reagent and RNA quality was evaluated with a Bioanalyzer 2100 (Agilent, CA, USA). cDNA library was created using high-quality RNA. In the end, an Illumina Novaseq 6000 was applied to carry out 2x150bp paired-end sequencing.

Bioinformatics analysis was completed by LC-Bio Technology (Hangzhou, China). Brief, fastp (https://github.com/OpenGene/fastp), HISAT2 (https://ccb.jhu.edu/software/hisat2), StringTie (https://ccb.jhu.edu/software/stringtie), Gffcompare (https://github.com/gpertea/gffcompare/) and R package edgeR (https://bioconductor.org/packages/release/bioc/html/edgeR.html) were used for various analyses. For Kyoto Encyclopedia of Genes and Genomes (KEGG) pathway enrichment analysis and gene-set enrichment analysis (GSEA), DAVID software (https://david.ncifcrf.gov/) and GSEA4.1.0 software (http://www.gsea-msigdb.org/gsea/index.jsp) were used, respectively.

2.12. Quantification and statistical analyses

All data in this study were presented as means ± SEM. Statistical analyses were carried out with unpaired Student's t test (Excel), or two-way ANOVA followed by Bonferroni's test (GraphPad Prism 9). $p < 0.05$ was considered statistically significant. We applied GraphPad Prism 9 and Adobe Illustrator 2020 to generate and prepare figures.

3. RESULTS

3.1. Generation of peroxidase-dead PRDX1 variant (PRDX1^{Cys52Ser}) mice

To investigate the *in vivo* role of PRDX1's peroxidase activity in the control of inflammation, we generated a peroxidase-dead PRDX1 variant (PRDX1^{Cys52Ser}) mouse strain through CRISPR-Cas9 approach by mutating the peroxidatic Cys52 to serine residue (Figure 1A) as confirmed by DNA sequencing analysis (Figure 1B). Since Cys52 is the key site mediating PRDX1's peroxidase activity [9], we assessed the peroxidase activity of global PRDX in the liver of PRDX1^{Cys52Ser} mice using a classical Trx-TrxR-NADPH coupled activity assay [24,27], where NADPH consumption rates indirectly reflect the peroxidase activity of global PRDX. As revealed by this activity assay, PRDX1^{Cys52Ser} variant mice showed significantly reduced global PRDX peroxidase activity compared with their wild-type (WT) littermates (Figure 1C).

Some PRDX members (PRDX1-3) could become hyperoxidized at their conserved peroxidatic cysteine owing to slow formation of disulfide between the peroxidatic cysteine and the resolving cysteine during a catalytic cycle [9]. Using a commercial antibody (Anti-Peroxiredoxin-SO3, ab16830, abcam) that is supposed to recognize the hyperoxidized forms of PRDX [28], we observed that PRDX1 hyperoxidation was drastically reduced in the liver of PRDX1^{Cys52Ser} mice (Figure 1D). Collectively, these results confirm that PRDX1^{Cys52Ser} variant mice are enzymatically inactive.

3.2. PRDX1^{Cys52Ser} variant mice were protected from western diet (WD)-induced NASH and liver fibrosis

We sought to evaluate the functional role of PRDX1 Cys52Ser in NASH by feeding both male and female WT and PRDX1^{Cys52Ser} mice a WD that is rich in fat and fructose as a common strategy to induce NASH experimental models [3]. Twenty20 weeks after WD feeding, compared with WT mice, PRDX1^{Cys52Ser} mice showed similar body weight (Figs. S1A and S1B), food intake (Fig. S1C) and energy expenditure (Fig. S1D). We also found no difference in the ratio of either fat mass or lean mass over body weight (Figs. S1E and S1F). Interestingly, however, PRDX1^{Cys52Ser} mice significantly reduced liver weight (Figure 2A, B) and the ratio of liver weight over body weight (Figs. S1G and S1H).

Serum levels of alanine aminotransferase (ALT) and aspartate aminotransferase (AST) that are indicative of liver injury [29], were significantly decreased in PRDX1^{Cys52Ser} mice compared with WT mice (Figure 2C, D), suggesting alleviated liver injury in PRDX1^{Cys52Ser} mice. We next carried out a series of histological staining in the liver including H&E, Oil-Red-O, Sirius Red and smooth muscle alpha-actin (α-SMA) to reflect the severity of NASH and liver fibrosis. Clearly, PRDX1^{Cys52Ser} mice reduced steatosis (Figs. S2A and S2B), lipid accumulation (Figure 2E, F), and liver fibrosis (Figure 2G, H, Figs. S2C and S2D).

Consistent with the observed NASH phenotypes, the expression levels of some pro-inflammatory (e.g. *Mcp-1*, *Cdllb*, *Cdllc*, *Tnf-α, Il-1β*) and fibrotic (e.g. *Pdgfa*, *Pdgfb*, *Pdgfra*, *Col1a1*, *Col3a1, Icam1*) genes were significantly reduced in the liver of PRDX1^{Cys52Ser} mice (Figure 2I, J). Interestingly, we observed no differences in the levels of hepatic H_2O_2 (Fig. S2E), as detected by HKPerox-Red, a selective H_2O_2 probe [26], and hepatic malondialdehyde (MDA) (Fig. S2F), a marker for lipid peroxidation [4], between male WT and PRDX1^{Cys52Ser} mice after WD,

 © 2023 The Authors. Published by Elsevier GmbH. This is an open access article under the CC BY-NC-ND license (http://creativecommons.org/licenses/by-nc-nd/4.0/).

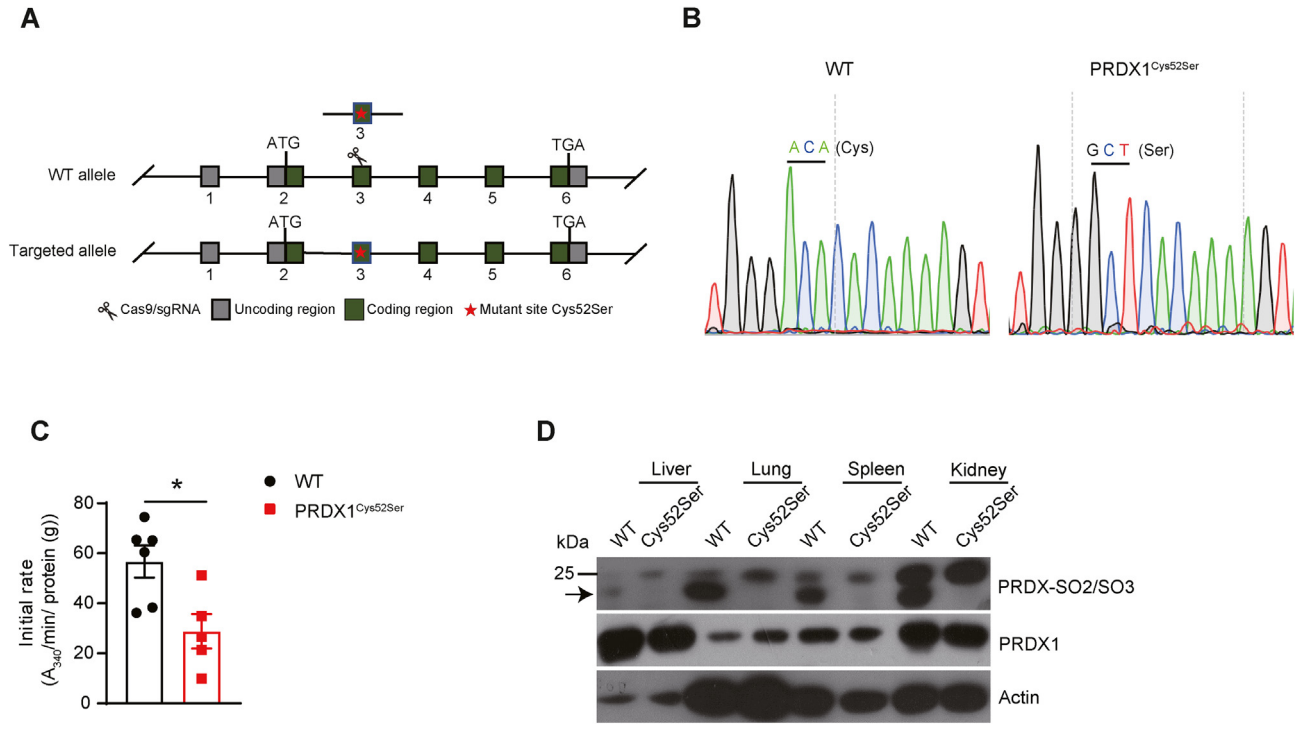

Figure 1: Generation and validation of PRDX1^{Cys52Ser} variant mice. **(A)** Schematic showing the generation of PRDX1^{Cys52Ser} variant mice, where the peroxidatic cysteine at 52 (Cys52) of PRDX1 was mutated to serine (Ser) via CRIPR-Cas9 system. **(B)** Validation of homozygous PRDX1^{Cys52Ser} variants via mouse genome DNA sequencing. **(C)** Global hepatic PRDX peroxidase activity in WT and PRDX1^{Cys52Ser} variant mice. Eight-week-old male mice on a chow diet were used to measure the peroxidase activity of global PRDX via a classical Trx-TrxR-NADPH coupled assay. Background activity was measured in samples without Trx and TrxR. The initial NADPH consumption rate (initial rate) was calculated by performing a simple linear regression using absorbance at 340 nm (A_{340}) readings during the first five minutes. The global PRDX peroxidase activity was calculated by subtracting the background activity (initial rate) from total activity (initial rate). WT mice (n = 6), PRDX1^{Cys52Ser} mice (n = 5). *p < 0.05 by student's *t*-test. **(D)** Hyperoxidation of PRDX in the various tissues detected by WB. A commercial antibody recognizing the hyperoxidized form (SO3) of PRDX was used to detect any changes in PRDX hyperoxidation between WT and PRDX1^{Cys52Ser} mice. The arrow denotes the potential hyperoxidized PRDX1 according to its molecular weight (22 kDa).

suggesting that PRDX1 peroxidase mutation does not alter the extent of oxidative stress in the liver. Taken together, these data indicate that PRDX1 Cys52Ser variant mitigates WD-induced NASH and liver fibrosis.

3.3. Downregulated NF-κB and JAK-STAT signaling pathways in PRDX1^{Cys52Ser} mice

To understand the signaling pathways accounting for alleviated NASH and liver fibrosis in PRDX1^{Cys52Ser} mice, we performed RNA sequencing (RNA-Seq) of liver samples from male WT and PRDX1^{Cys52Ser} mice after WD. Heatmaps showed a significant decrease of genes related to inflammation (Fig. S3A), fibrosis (Fig. S3B), and specifically to NF-κB signaling (Figure 3A) and JAK-STAT signaling (Figure 3B) pathways in PRDX1^{Cys52Ser} mice. Consistently, both gene-set enrichment analysis (GSEA) and Kyoto Encyclopedia of Genes and Genomes (KEGG) showed an enrichment of differentially expressed genes related to NF-κB signaling or JAK-STAT signaling pathway (Figure 3C, D, Fig. S3C). In addition, volcano plots indicated the significantly downregulated genes related to NF-κB signaling or JAK-STAT signaling pathway in PRDX1^{Cys52Ser} mice (Figs. S3D and S3E).

Using qPCR, we further verified the significantly reduced expression of some genes related to NF-κB signaling or JAK-STAT signaling pathway in PRDX1^{Cys52Ser} mice (Figure 3E). Taken together, these data provide evidence supporting that NF-κB and JAK-STAT signaling pathways were downregulated in the liver of PRDX1^{Cys52Ser} mice.

3.4. PRDX1 Cys52Ser variant reduced the signaling activity of hepatic NF-κB and STAT1

Numerous studies have well established NF-κB as a central player in stimulating inflammatory response [30], and one previous study has shown that activation of STAT1 and STAT3 promotes obesity-associated NASH and hepatocellular carcinoma, respectively [31]. Our RNA-Seq and qPCR results have indicated a significant decrease in NF-κB and JAK-STAT signaling pathways in PRDX1^{Cys52Ser} mice. Therefore, we next evaluated the signaling activities of NF-κB and STAT1. The phosphorylation levels of both NF-κB and STAT1 were significantly reduced in the liver of PRDX1^{Cys52Ser} mice after WD (Figure 3F, G).

We next sought to test for a causal link between PRDX1 Cys52Ser variant and reduced inflammation. First, we treated 8-week-old male WT and PRDX1^{Cys52Ser} mice on normal chow diet with lipopolysaccharide (LPS). As shown in Figure 3H, LPS-induced NF-κB p65 phosphorylation in the liver was significantly reduced in PRDX1^{Cys52Ser} mice compared with WT mice. Second, using primary hepatocytes isolated from chow-fed 6-week-old male WT and PRDX1^{Cys52Ser} mice, we observed that LPS-induced NF-κB p65 phosphorylation (Fig. S3F) and expression of some pro-inflammatory genes (*Il-6*, *Cxcl1* and *Mcp-1*) (Fig. S3G) were significantly reduced in PRDX1^{Cys52Ser} hepatocytes compared with WT hepatocytes. These results collectively demonstrate that PRDX1 Cys52Ser variant inhibits the NF-κB signaling activity and the pro-inflammatory response in the liver.

 © 2023 The Authors. Published by Elsevier GmbH. This is an open access article under the CC BY-NC-ND license (http://creativecommons.org/licenses/by-nc-nd/4.0/).

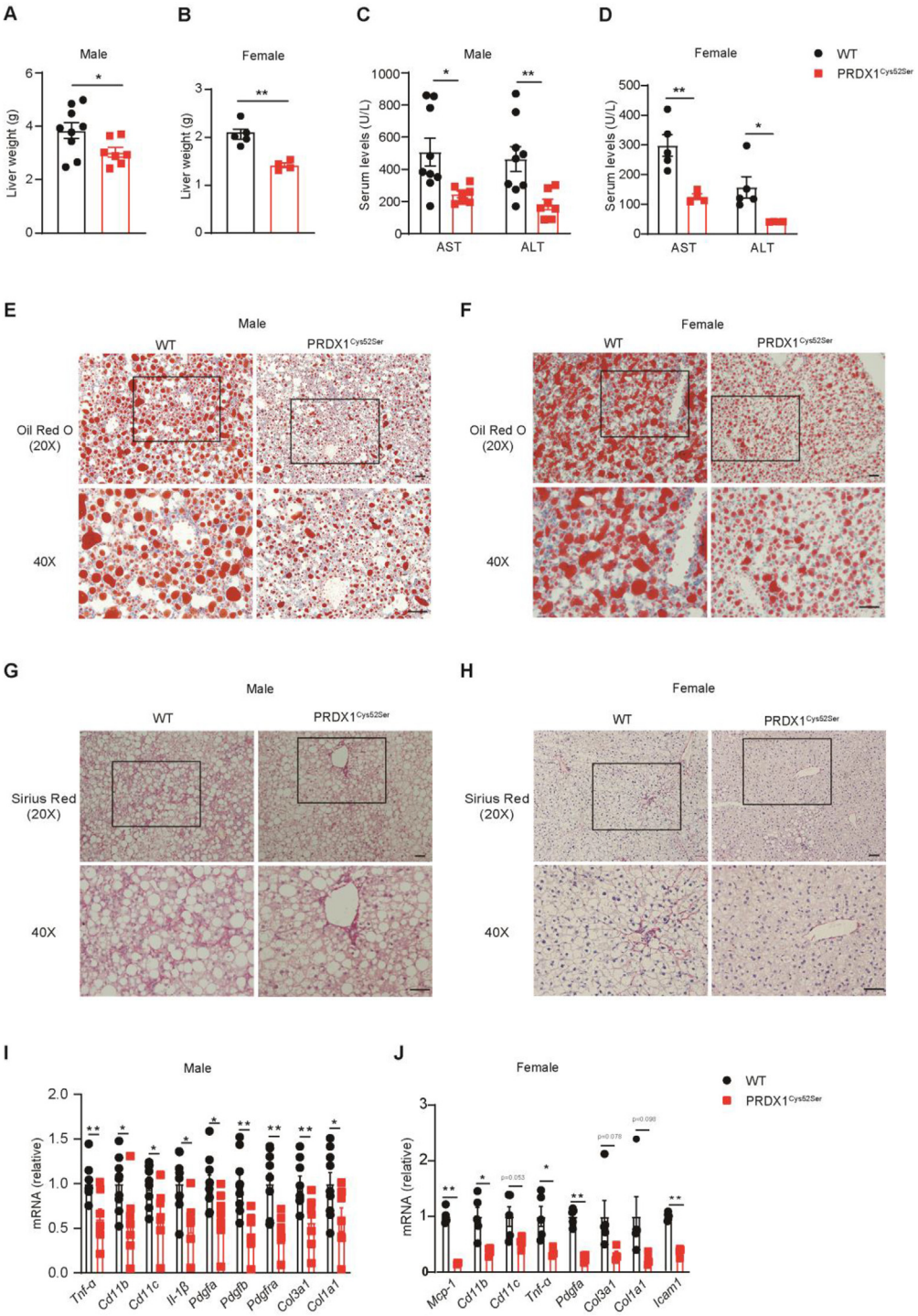

Figure 2: PRDX1^{Cys52Ser} variants are protected from WD-induced NASH and liver fibrosis. **(A and B)** Liver weights of male (A) or female (B) WT and PRDX1^{Cys52Ser} mice after WD feeding. Eight-week-old mice were fed a WD for a total of 20 weeks before their blood and liver samples were collected for subsequent analyses including serum measurement, histological staining, WB and qPCR. Male WT mice (n = 9), male PRDX1^{Cys52Ser} mice (n = 7); female WT mice (n = 5), female PRDX1^{Cys52Ser} mice (n = 4). *p < 0.05, **p < 0.01 by Student's *t* test. **(C and D)** Serum levels of aspartate aminotransferase (AST) and alanine aminotransferase (ALT) in male (C) or female (D) WT and PRDX1^{Cys52Ser} mice after WD feeding (as in A and B). Male WT mice (n = 9), male PRDX1^{Cys52Ser} mice (n = 7); female WT mice (n = 5), female PRDX1^{Cys52Ser} mice (n = 4). *p < 0.05, **p < 0.01 by Student's *t* test. **(E and F)** Representative images from 3 mice per group showing Oil Red O staining of liver tissues from male (E) or female (F) WT and PRDX1^{Cys52Ser} mice after WD feeding (as in A and B). Scale bars, 50 μm. **(G and H)** Representative images from 3 mice per group showing Sirius Red staining of liver tissues from male (G) or female (H) WT and PRDX1^{Cys52Ser} mice after WD feeding (as in A and B). Scale bars, 50 μm. **(I and J)** mRNA levels of pro-inflammatory or fibrotic genes in the liver of male (I) or female (J) WT and PRDX1^{Cys52Ser} mice after WD feeding (as in A and B). Male WT mice (n = 9), male PRDX1^{Cys52Ser} mice (n = 7); female WT mice (n = 5), female PRDX1^{Cys52Ser} mice (n = 4). *p < 0.05, **p < 0.01 by Student's *t* test. See also Figs. S1 and S2. All data are presented as means ± SEM.

 © 2023 The Authors. Published by Elsevier GmbH. This is an open access article under the CC BY-NC-ND license (http://creativecommons.org/licenses/by-nc-nd/4.0/).

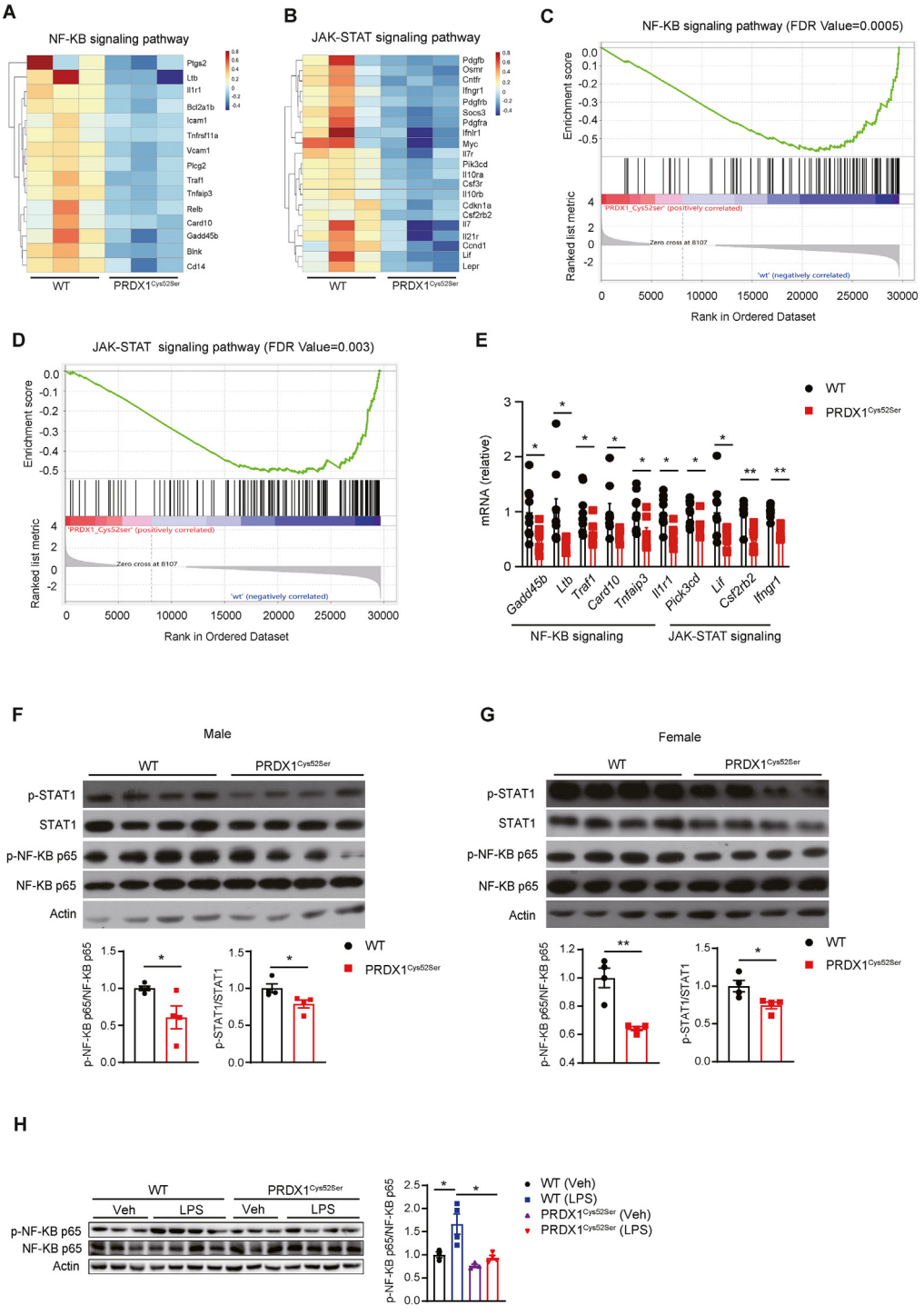

Figure 3: Reduced NF-κB signaling and STAT1 signaling pathways in the liver of PRDX1^{Cys52Ser} mice after WD feeding. **(A)** Heatmap showing the significantly decreased expression of genes related to NF-κB signaling pathway in the liver of male PRDX1^{Cys52Ser} mice after WD. Eight-week-old male WT and PRDX1^{Cys52Ser} mice were fed a WD for 20 weeks before their liver tissues were collected for RNA-Seq and subsequent bioinformatics analyses. **(B)** Heatmap showing the significantly decreased genes related to JAK-STAT signaling pathway (as in A). **(C and D)** Gene-set enrichment analysis (GSEA) showing an enrichment of differentially expressed genes related to NF-κB signaling (C) or JAK-STAT signaling (D) pathway. **(E)** Expression of genes related to NF-κB or JAK-STAT signaling pathways in the liver (as in A). **(F and G)** Western blotting and quantitative analysis of hepatic NF-κB and STAT1 signaling activities in male (F) or female (G) WT and PRDX1^{Cys52Ser} mice after 20 weeks of WD. n = 4 mice per group. *p < 0.05, **p < 0.01 by Student's *t* test. **(H)** WB of hepatic NF-κB signaling activity in WT and PRDX1^{Cys52Ser} mice treated with LPS and quantification. Eight-week-old male mice on chow diet were intraperitoneally injected with LPS (10 mg/kg) for 15 min before their liver samples were collected for WB analysis. Veh, vehicle; LPS, lipopolysaccharide. WT mice (n = 3 for Veh treatment; n = 4 for LPS treatment), PRDX1^{Cys52Ser} mice (n = 3 for Veh treatment; n = 4 for LPS treatment); *p < 0.05 by one-way ANOVA followed by Bonferroni's test. See also Fig. S3. All data are presented as means ± SEM.

 © 2023 The Authors. Published by Elsevier GmbH. This is an open access article under the CC BY-NC-ND license (http://creativecommons.org/licenses/by-nc-nd/4.0/).

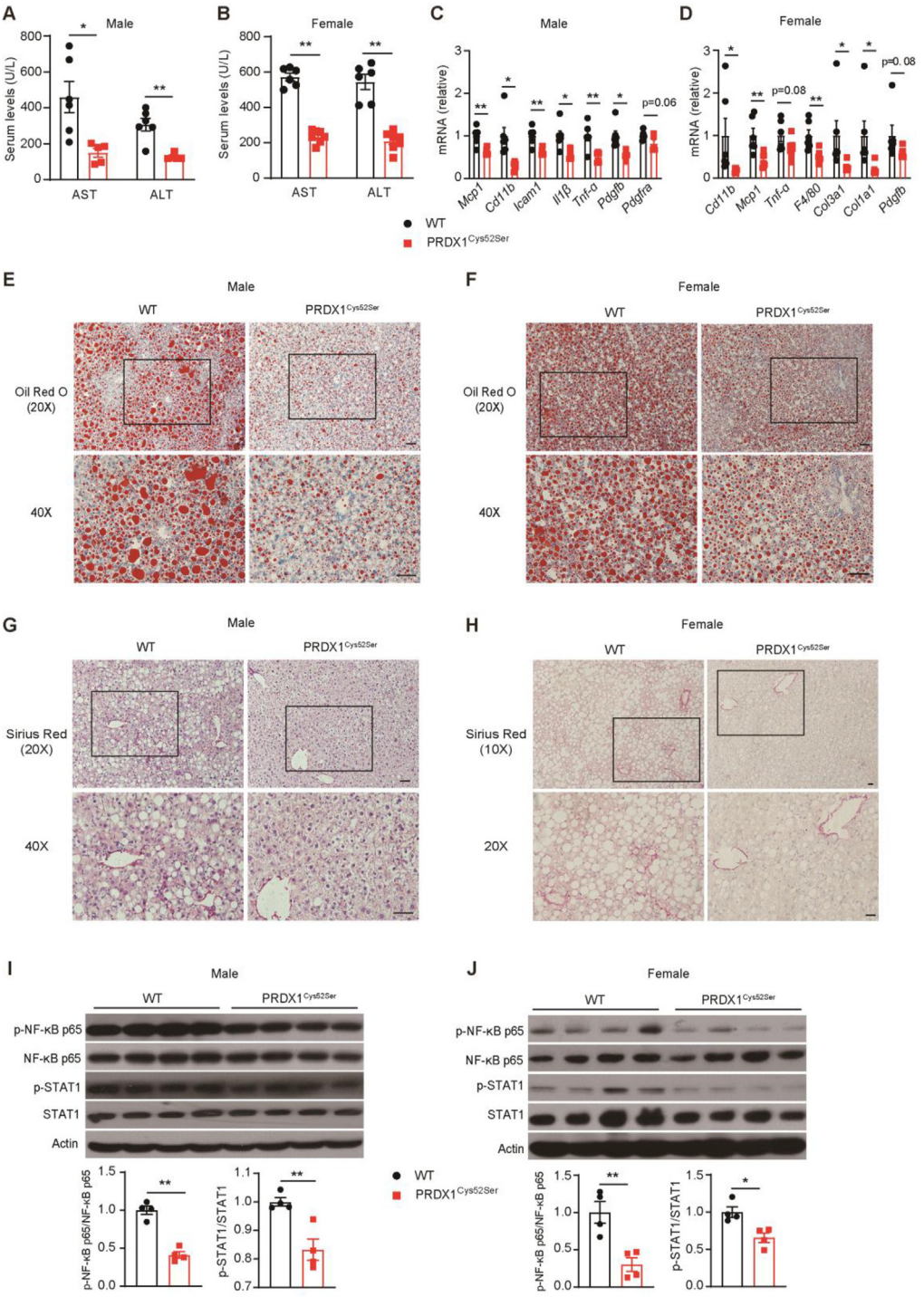

Figure 4: PRDX1 Cys52Ser variant confers resistance to MCD-induced NASH and liver fibrosis by suppressing NF-κB and STAT1 signaling activities. **(A and B)** Serum levels of AST and ALT in male (A) or female (B) WT and PRDX1^{Cys52Ser} mice after MCD feeding. Eight-week-old mice were fed a MCD for 5 weeks before their blood and liver samples were collected for subsequent analyses. Male WT mice (n = 6), male PRDX1^{Cys52Ser} mice (n = 5); female WT mice (n = 6), female PRDX1^{Cys52Ser} mice (n = 7). *p < 0.05, **p < 0.01 by Student's *t* test. **(C and D)** mRNA levels of pro-inflammatory or fibrotic genes in the livers of male (C) or female (D) WT and PRDX1^{Cys52Ser} mice (as in A and B). Male WT mice (n = 6), male PRDX1^{Cys52Ser} mice (n = 5); female WT mice (n = 6), female PRDX1^{Cys52Ser} mice (n = 7). *p < 0.05, **p < 0.01 by Student's *t* test. **(E and F)** Representative images from 3 mice per group showing Oil Red O staining of liver tissues from male (E) or female (F) WT and PRDX1^{Cys52Ser} mice (as in A and B). **(G and H)** Representative images from 3 mice per group showing Sirius Red staining of liver tissues from male (G) or female (H) WT and PRDX1^{Cys52Ser} mice (as in A and B). Scale bars, 50 μm. **(I and J)** Activities of hepatic NF-κB and STAT1 signaling in the liver of male (I) or female (J) WT and PRDX1^{Cys52Ser} mice after MCD feeding (as in A and B). n = 4 mice per group. *p < 0.05, **p < 0.01 by Student's *t* test. See also Fig. S4. All data are presented as means ± SEM.

 © 2023 The Authors. Published by Elsevier GmbH. This is an open access article under the CC BY-NC-ND license (http://creativecommons.org/licenses/by-nc-nd/4.0/).

3.5. PRDX1 Cys52Ser variant conferred resistance to methionine and choline deficiency diet (MCD)-induced NASH by suppressing NF-kB and STAT1 signaling pathways

MCD feeding is another common strategy to induce NASH experimental models without obesity and insulin resistance [3]. We tested the potential effect of PRDX1 Cys52Ser variant on MCD-induced NASH. After 5 weeks of MCD feeding, PRDX1^{Cys52Ser} mice showed comparable body weight (Figs. S4A and S4B), liver weight (Figs. S4C and S4D), and the ratio of liver weight over body weight (Figs. S4E and S4F), but significantly lower serum levels of AST and ALT than WT mice (Figure 4A, B).

The expression of some genes related to inflammation and fibrosis (*Mcp-1, F4/80, Cd11b, Col1a-1* and *Col3a1*) was significantly reduced in the liver of PRDX1^{Cys52Ser} mice (Figure 4C, D), suggesting the alleviated NASH phenotype. Indeed, histological staining including H&E, Oil Red O, Sirius Red and α-SMA staining showed a drastic decrease in hepatic lipid accumulation (Figure 4E, F, Figs. S4G and S4H) and liver fibrosis (Figure 4G, H, Figs. S4I and S4J) in PRDX1^{Cys52Ser} mice.

We further observed that the signaling activities of STAT1 and NF-κB were significantly reduced in the liver of PRDX1^{Cys52Ser} mice (Figure 4I, J). Collectively, these results have demonstrated that PRDX1 Cys52Ser variant confers resistance to MCD-induced NASH and liver fibrosis by suppressing hepatic NF-κB and STAT1 signaling pathways.

4. DISCUSSION

In this study, we tried to address an interesting question regarding the reported pro-inflammatory effect of PRDX1 that simultaneously shows potent antioxidant activity as a peroxidase. By generating PRDX1^{Cys52Ser} variant mice, we had an opportunity to investigate how PRDX1 enzymatic function impacts its pro-inflammatory activity. Our results have clearly demonstrated that inflammation and liver fibrosis are markedly reduced in PRDX1^{Cys52Ser} mice on either WD or MCD. Thus, our study provides *in vivo* evidence supporting a link of PRDX1's peroxidase activity with its pro-inflammatory activity. In line with our study, one previous *in vitro* study suggested the dependence of PRDX1's pro-inflammatory effect on its peroxidatic or resolving cysteine mediating its peroxidase activity [19].

How PRDX1 Cys52Ser variant suppresses inflammation mechanistically remains elusive yet. Previous studies have demonstrated that extracellular PRDX1 stimulates inflammatory responses by binding to TLR4 [32], and mutation of peroxidatic Cys52 of PRDX1 inhibits its extracellular release as a chaperone protein in response to TNF-α [19], suggesting that PRDX1 Cys52 is required for its chaperone function in promoting inflammatory response. In support of an inflammation-promoting role for PRDX1 Cys52, we found that expression of various pro-inflammatory genes and NF-κB signaling activity were markedly reduced in PRDX1^{Cys52Ser} variant mice. It should be noted that these previous studies were mainly carried out in cultured cells. Whether or not PRDX1 Cys52Ser variant blocks its extracellular release *in vivo* remains to be investigated. In addition, we also postulate that PRDX1 Cys52Ser variant may inhibit the pro-inflammatory response by interacting with some molecules involved in the pro-inflammatory signaling pathways. Yet, future studies are required to fully understand how PRDX1 Cys52Ser variant suppresses the activation of NF-κB signaling mechanistically.

Some studies have suggested that the chaperone function of PRDX depends on their oligomerization (e.g., dimerization, decamerization) or hyperoxidation [18,19,33]. The peroxidatic Cys52 is critical for PRDX1 dimerization or hyperoxidation [9]. Consistently, we observed reduced PRDX1 hyperoxidation and inflammation in PRDX1^{Cys52Ser} mice, demonstrating that the pro-inflammatory activity of PRDX1 is dependent of its Cys52.

Inflammation and anti-oxidation are two opposing forces in the pathogenesis of NASH, and PRDX1 possesses these two opposing activities, implicating a complex role for PRDX1 in NASH. Although we demonstrate that PRDX1 Cys52 is required for its pro-inflammatory effect, whether or not PRDX1's pro-inflammatory activity influences its peroxidase activity is unknown. Overall, our study suggests that in the physiological settings, inactive PRDX1 dimer is reduced by Trx efficiently and sufficiently to active PRDX1 monomer that protects against oxidative stress by functioning as a potent peroxidase; whereas in the pathogenesis of NASH, dimerized or hyperoxidized PRDX1 due to overwhelming oxidants might not be reduced by Trx efficiently, consequently promoting inflammation by functioning as a chaperone protein.

5. CONCLUSIONS

PRDX1 Cys52Ser variant confers resistance to NASH and liver fibrosis in mice by reducing NF-κB and STAT1 signaling pathways, suggesting that PRDX1 exerts dual but opposing roles in NASH.

AUTHOR CONTRIBUTIONS

XX conceived and supervised the project, analyzed and interpreted the data, and wrote the manuscript. ZB performed physiological measurements of mice, WB, qPCR and histological staining of liver samples. WY did histological staining of liver samples, isolated primary mouse hepatocytes, and measured PRDX peroxidase activity as well as serum levels of AST and ALT. RL performed qPCR analysis. MT conducted WB and qPCR analyses. XS discussed and analyzed the data. CL discussed and interpreted the data.

DECLARATION OF COMPETING INTEREST

The authors declare that no conflict of interest exists.

DATA AVAILABILITY

The RNAseq data generated in this study have been deposited in GEO (GSE240198).

ACKNOWLEDGEMENTS

We thank Prof. Dan Yang at Westlake University for providing us with the HKPerox-Red probe, all laboratory members for their critical comments on the manuscript, and GemPharmatech (Nanjing, China) for generation of PRDX1^{Cys52Ser} variant mice. This work was supported by the National Key Research and Development Program of China (2019YFA0802500 to X.X.), the National Natural Science Foundation of China (31971076, 32271202 to X.X.), the Tianjin Municipal Science and Technology Commission (20JCJQJC00240 to X.X.), and the Tianjin Key Medical Discipline (Specialty) Construction Project (TJYXZDXK-032A).

APPENDIX A. SUPPLEMENTARY DATA

Supplementary data to this article can be found online at https://doi.org/10.1016/j.molmet.2023.101789.

 © 2023 The Authors. Published by Elsevier GmbH. This is an open access article under the CC BY-NC-ND license (http://creativecommons.org/licenses/by-nc-nd/4.0/).

REFERENCES

[1] Loomba R, Friedman SL, Shulman GI. Mechanisms and disease consequences of nonalcoholic fatty liver disease. Cell 2021;184(10):2537–64.

[2] Musso G, Cassader M, Gambino R. Non-alcoholic steatohepatitis: emerging molecular targets and therapeutic strategies. Nat Rev Drug Discov 2016;15(4):249–74.

[3] Friedman SL, Neuschwander-Tetri BA, Rinella M, Sanyal AJ. Mechanisms of NAFLD development and therapeutic strategies. Nat Med 2018;24(7):908–22.

[4] Chen Z, Tian R, She Z, Cai J, Li H. Role of oxidative stress in the pathogenesis of nonalcoholic fatty liver disease. Free Radic Biol Med 2020;152:116–41.

[5] Pafili K, Roden M. Nonalcoholic fatty liver disease (NAFLD) from pathogenesis to treatment concepts in humans. Mol Metab 2021;50:101122.

[6] Chae HZ, Robison K, Poole LB, Church G, Storz G, Rhee SG. Cloning and sequencing of thiol-specific antioxidant from mammalian brain: alkyl hydroperoxide reductase and thiol-specific antioxidant define a large family of antioxidant enzymes. Proc Natl Acad Sci U S A 1994;91(15):7017–21.

[7] Perkins A, Nelson KJ, Parsonage D, Poole LB, Karplus PA. Peroxiredoxins: guardians against oxidative stress and modulators of peroxide signaling. Trends Biochem Sci 2015;40(8):435–45.

[8] Wood ZA, Poole LB, Karplus PA. Peroxiredoxin evolution and the regulation of hydrogen peroxide signaling. Science 2003;300(5619):650–3.

[9] Rhee SG, Kil IS. Multiple functions and regulation of mammalian peroxiredoxins. Annu Rev Biochem 2017;86:749–75.

[10] Chae HZ, Chung SJ, Rhee SG. Thioredoxin-dependent peroxide reductase from yeast. J Biol Chem 1994;269(44):27670–8.

[11] Cao J, Schulte J, Knight A, Leslie NR, Zagozdzon A, Bronson R, et al. Prdx1 inhibits tumorigenesis via regulating PTEN/AKT activity. EMBO J 2009;28(10):1505–17.

[12] Ahmed W, Lingner J. PRDX1 and MTH1 cooperate to prevent ROS-mediated inhibition of telomerase. Genes Dev 2018;32(9–10):658–69.

[13] Kisucka J, Chauhan AK, Patten IS, Yesilaltay A, Neumann C, Van Etten RA, et al. Peroxiredoxin1 prevents excessive endothelial activation and early atherosclerosis. Circ Res 2008;103(6):598–605.

[14] Bae SH, Sung SH, Cho EJ, Lee SK, Lee HE, Woo HA, et al. Concerted action of sulfiredoxin and peroxiredoxin I protects against alcohol-induced oxidative injury in mouse liver. Hepatology 2011;53(3):945–53.

[15] He Y, Li S, Tang D, Peng Y, Meng J, Peng S, et al. Circulating Peroxiredoxin-1 is a novel damage-associated molecular pattern and aggravates acute liver injury via promoting inflammation. Free Radic Biol Med 2019;137:24–36.

[16] Chang JW, Lee SH, Jeong JY, Chae HZ, Kim YC, Park ZY, et al. Peroxiredoxin-I is an autoimmunogenic tumor antigen in non-small cell lung cancer. FEBS Lett 2005;579(13):2873–7.

[17] Shichita T, Hasegawa E, Kimura A, Morita R, Sakaguchi R, Takada I, et al. Peroxiredoxin family proteins are key initiators of post-ischemic inflammation in the brain. Nat Med 2012;18(6):911–7.

[18] Moon JC, Hah YS, Kim WY, Jung BG, Jang HH, Lee JR, et al. Oxidative stress-dependent structural and functional switching of a human 2-Cys peroxiredoxin isotype II that enhances HeLa cell resistance to H2O2-induced cell death. J Biol Chem 2005;280(31):28775–84.

[19] Mullen L, Hanschmann EM, Lillig CH, Herzenberg LA, Ghezzi P. Cysteine oxidation targets peroxiredoxins 1 and 2 for exosomal release through a novel mechanism of redox-dependent secretion. Mol Med 2015;21(1):98–108.

[20] Su W, Wu S, Yang Y, Guo Y, Zhang H, Su J, et al. Phosphorylation of 17beta-hydroxysteroid dehydrogenase 13 at serine 33 attenuates nonalcoholic fatty liver disease in mice. Nat Commun 2022;13(1):6577.

[21] Fuchs CD, Radun R, Dixon ED, Mlitz V, Timelthaler G, Halilbasic E, et al. Hepatocyte-specific deletion of adipose triglyceride lipase (adipose triglyceride lipase/patatin-like phospholipase domain containing 2) ameliorates dietary induced steatohepatitis in mice. Hepatology 2022;75(1):125–39.

[22] Xie X, Yang H, An JJ, Houtz J, Tan JW, Xu H, et al. Activation of anxiogenic circuits instigates resistance to diet-induced obesity via increased energy expenditure. Cell Metab 2019;29(4):917–931 e914.

[23] Mansuy-Aubert V, Zhou QL, Xie X, Gong Z, Huang JY, Khan AR, et al. Imbalance between neutrophil elastase and its inhibitor alpha1-antitrypsin in obesity alters insulin sensitivity, inflammation, and energy expenditure. Cell Metab 2013;17(4):534–48.

[24] Kim JA, Park S, Kim K, Rhee SG, Kang SW. Activity assay of mammalian 2-cys peroxiredoxins using yeast thioredoxin reductase system. Anal Biochem 2005;338(2):216–23.

[25] Xie X, Gong Z, Mansuy-Aubert V, Zhou QL, Tatulian SA, Sehrt D, et al. C2 domain-containing phosphoprotein CDP138 regulates GLUT4 insertion into the plasma membrane. Cell Metab 2011;14(3):378–89.

[26] Ye S, Hu JJ, Zhao QA, Yang D. Fluorescent probes for in vitro and in vivo quantification of hydrogen peroxide. Chem Sci 2020;11(44):11989–97.

[27] Nelson KJ, Parsonage D. Measurement of peroxiredoxin activity. Curr Protoc Toxicol 2011. Chapter 7:Unit7 10.

[28] Woo HA, Kang SW, Kim HK, Yang KS, Chae HZ, Rhee SG. Reversible oxidation of the active site cysteine of peroxiredoxins to cysteine sulfinic acid. Immunoblot detection with antibodies specific for the hyperoxidized cysteine-containing sequence. J Biol Chem 2003;278(48):47361–4.

[29] Bjornsson E, Nordlinder H, Olsson R. Clinical characteristics and prognostic markers in disulfiram-induced liver injury. J Hepatol 2006;44(4):791–7.

[30] Taniguchi K, Karin M. NF-kappaB, inflammation, immunity and cancer: coming of age. Nat Rev Immunol 2018;18(5):309–24.

[31] Grohmann M, Wiede F, Dodd GT, Gurzov EN, Ooi GJ, Butt T, et al. Obesity drives STAT-1-dependent NASH and STAT-3-dependent HCC. Cell 2018;175(5):1289–1306 e1220.

[32] Riddell JR, Wang XY, Minderman H, Gollnick SO. Peroxiredoxin 1 stimulates secretion of proinflammatory cytokines by binding to TLR4. J Immunol 2010;184(2):1022–30.

[33] Saccoccia F, Di Micco P, Boumis G, Brunori M, Koutris I, Miele AE, et al. Moonlighting by different stressors: crystal structure of the chaperone species of a 2-Cys peroxiredoxin. Structure 2012;20(3):429–39.

 © 2023 The Authors. Published by Elsevier GmbH. This is an open access article under the CC BY-NC-ND license (http://creativecommons.org/licenses/by-nc-nd/4.0/).